Molecular dynamics simulations of the effect of adsorption on SiO2 surfaces

D. C. Athanasopoulos and S. H. Garofalini

Citation: The Journal of Chemical Physics **97**, 3775 (1992); doi: 10.1063/1.462958
View online: http://dx.doi.org/10.1063/1.462958
View Table of Contents: http://scitation.aip.org/content/aip/journal/jcp/97/5?ver=pdfcov
Published by the AIP Publishing

Molecular dynamics simulations of the effect of adsorption on SiO_2 surfaces

D. C. Athanasopoulos and S. H. Garofalini
Department of Ceramics and Interfacial Molecular Science Laboratory, Institute for Engineered Materials, Rutgers University, Piscataway, New Jersey 08855

(Received 10 April 1992; accepted 14 May 1992)

Molecular dynamics computer simulations were used to study the adsorption of model Pt on silica and the effect of this adsorption on the structure of the silica surface. Silica glass and amorphized crystalline surfaces were used as the silica substrates. Results showed a 5–6 Å thick adsorbate/substrate interface and an approximately 1 Å compression of the substrate surface caused by the presence of the adsorbate film. A significant decrease in the Si–O–Si bond-angle distribution was observed as a result of the adsorption. The shift to smaller bond angles was caused by a distortion of the siloxane bonds in five- and six-membered rings rather than the formation of small sized rings. The smaller bond angles indicate that more reactive sites may exist in the surface.

INTRODUCTION

The deposition of metals on oxide surfaces has been studied using both experimental and computational techniques.[1–8] These interfaces play an important role in a wide variety of technological applications, such as heterogeneous supported catalysts,[9] thin film technology, and high-density integrated circuit technology. The metal/oxide interactions determine the penetration depth of the metal inside the oxide and the adhesion of the formed metal film on the surface. Since the metals are approaching the oxide surface from the gas phase, the metal–metal interactions are negligible in the beginning and the metal-substrate interactions dominate the deposition process. When the concentration of metals at the surface becomes enough for the metal–metal interactions to contribute to the energetics of adsorption, the situation changes. At that time global effects associated with the deposition rate and the substrate structure influence the structure of the interface. The molecular dynamics (MD) computer simulation technique becomes an important probe for the understanding of this process because, with the employment of proper interatomic interaction potentials, it can provide data concerning more collective aspects of the metal-oxide system without further assumptions.

The results of computer simulations of the deposition of model Pt on silica glass surfaces are presented in this paper. Results of previous calculations of similar depositions have already been published.[2,10,11] In the present calculations, improved interatomic potentials which contain three-body interactions for the glass are used. In addition, this study focuses on the modifications that the deposited atoms cause to the glass surface.

In an effort to eliminate any accidental dependence of the deposition pattern on the initial topography of the surface, Pt atoms were deposited on five different silica glass surfaces. The simulations were also repeated using quartz and cristobalite surfaces which showed significant reconstruction. The crystal surfaces were used to create surfaces which had different ring size distributions than that found in the amorphous silica case. The modifications of the substrate caused by the deposition of the Pt atoms were studied, in which the structure of the surface can be viewed as the varying parameter.

COMPUTATIONAL PROCEDURE

The deposition of Pt atoms on various silica surfaces was simulated using molecular dynamics computer simulations. Newton's classical equations of motion were numerically integrated using a fifth-order Nordsieck–Gear algorithm.[12] The time step was 1.0×10^{-3} ps.

A multibody potential designed for silica[13] and used for a wide variety of silicates[14–19] was used to describe the interactions among the substrate species. The multibody potential contains both two- and three-body terms. The pair potential is a modified Born–Mayer–Huggins (BMH) potential given as (see Table I)

$$v_{ij}=A_{ij}\exp(-r_{ij}/\rho_{ij})+Q_iQ_j\operatorname{erfc}(r_{ij}/\beta_{ij})/r_{ij}\,.$$

The dispersion terms are omitted from this form of the BMH potential. The first term represents the short-range core repulsion. The second term represents screened Coulomb interactions. The complementary error function reduces the full formal ionic charges, Q_i and Q_j, to lower, more accurate values as a function of distance between the pair of ions.[20,21] The constant β_{ij} is treated as a size-independent interaction-dependent parameter.

To allow for the partial covalency of silica, a three-body term was included in the potential. The form of this three-body potential was introduced by Stillinger and Weber for silicon.[22] Feuston and Garofalini[13] properly modified this potential for use in silica systems so that it gave good agreement between MD results and x-ray and neutron diffraction experiments. It has subsequently been applied to a variety of silicates, from molecular systems to bulk and surface systems, as mentioned earlier, all with excellent results. The form of this three-body term is

 0021-9606/92/173775-06$006.00

TABLE I. Parameters for the pair term in the modified BMH potential.

Atom pair	A_{ij} (10^{-8} ergs)	β_{ij} (Å)
Si–Si	0.1877	2.30
Si–O	0.2962	2.34
O–O	0.0725	2.34

$$v_{jik}(r_{ij},r_{ik},\theta_{jik}) = \lambda_{jik}\exp[\gamma_{ij}/(r_{ij}-r_i^c)-\gamma_{ik}/(r_{ik}-r_i^c)] \times (\cos\theta_{jik}+\cos\theta_{jik}^e)^2.$$

This potential penalizes the binding energy of any neighboring triplet of the substrate atoms whenever the angle θ_{jik}, which is subtended by r_{ij} and r_{ik}, deviates from the tetrahedral angle (109.471). The tendency of the central atom to retain the tetrahedral structure is adjusted by the parameter λ_{jik}. Since all the sp^3 orbitals of Si are bonded while O has two lone pairs of electrons, the value $\lambda_{\text{O-Si-O}}$ is much higher than that of $\lambda_{\text{Si-O-Si}}$. The effective distance cutoffs r_i^c are slightly shorter than the same nearest-neighbors separations in the O–O and Si–Si radial distribution functions, calculated from diffraction experiments. The values for the three-body parameters are given in Table II. Although the λ values are slightly different than those presented earlier,[13] the simulation results vary insignificantly.

The interaction between Pt atoms and between Pt and substrate atoms were described by using the Lennard-Jones (LJ) 12-6 pair potential. The parameters for the Pt–Pt, Pt–O, and Pt–Si have been previously adjusted[2,11,23] to result in a good agreement with structural and dynamic experimental results. Table III gives the LJ parameters in which the Pt–Pt and Pt–O ϵ values are nearly the same and Pt–Si is about half the strength of the others. Five different glass surfaces containing 648 ions, part of the group previously studied by Feuston and Garofalini,[15] were used in the simulation. An MD melt-quench technique was used for the preparation of the bulk silica glass and surface. The bulk systems, 21.4 Å in X, Y, and Z at 300 K, were melted and slowly cooled to 300 K. The formation of the free surface was accomplished by removing the periodic boundary condition in one dimension (Z) and freezing a bottom layer of atoms. After their formation, the glass surface systems were annealed by heating the mobile atoms to 1000 K and then cooling them gradually to 300 K. This last step simulates the spontaneous heating that occurs in the tip of the crack during fracture. Details of the formation of the glass surfaces have been previously published.[15] The different regions in the silica glass surface systems are shown in Fig. 1.

TABLE II. Parameters for three-body potential.

Atom triple	r_i^c (Å)	λ_i (10^{-11} ergs)	γ_i (Å)
Si–O–Si	2.6	1.0	2.0
O–Si–O	3.0	24.0	2.8

TABLE III. Parameters for Lennard-Jones potential.

Atom pair	ϵ_{ij} (10–11 ergs)	σ_{ij} (Å)
Pt–Si	0.04800	1.844
Pt–O	0.11166	1.809
Pt–Pt	0.10919	2.540

In addition to the glass surfaces, (001) cristobalite and quartz surfaces were prepared from the bulk crystals containing 576 atoms in dimensions $19.8\times19.8\times20.7$ Å and $19.7\times17.0\times21.6$ Å, respectively. Each corresponding bulk crystal lattice at room temperature (300 K) was simulated using a run with 5000 equilibration MD steps followed by 5000 constant energy MD steps. The bulk crystalline forms of silica are stable with the multibody potential used here. After this run, the periodic boundary condition along the z axis was removed, in which the bottom 200 atoms were frozen. Each system was subsequently heated to 600 K and then immediately quenched to room temperature using the same equilibration-constant energy MD run as was done for the initial bulk.

Although the bulk crystals are stable in the simulations, the crystal surfaces reconstructed significantly during heating such that they may be considered amorphized. The (001) surface was not assumed to be stable cleavage planes for these crystals. Rather, the surface plane was only used to create a surface which would have a structure which was different than the glass surfaces in a particular way. Specifically, the bulk crystal would have a more narrow ring size distribution than the bulk glass; this would restrict the final ring size distribution at the amorphized surface. Figure 2 shows the ring size distribution of five 3 Å wide layers for the cristobalite system as a function of the distance of the layer from the surface (first layer is at the outer surface, fifth layer is in the interior). The two deepest layers contain exclusively six-membered rings, as

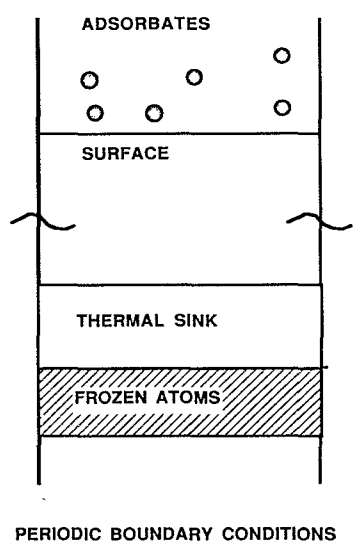

FIG. 1. Schematic diagram of the different regions in the molecular-dynamics computational cell.

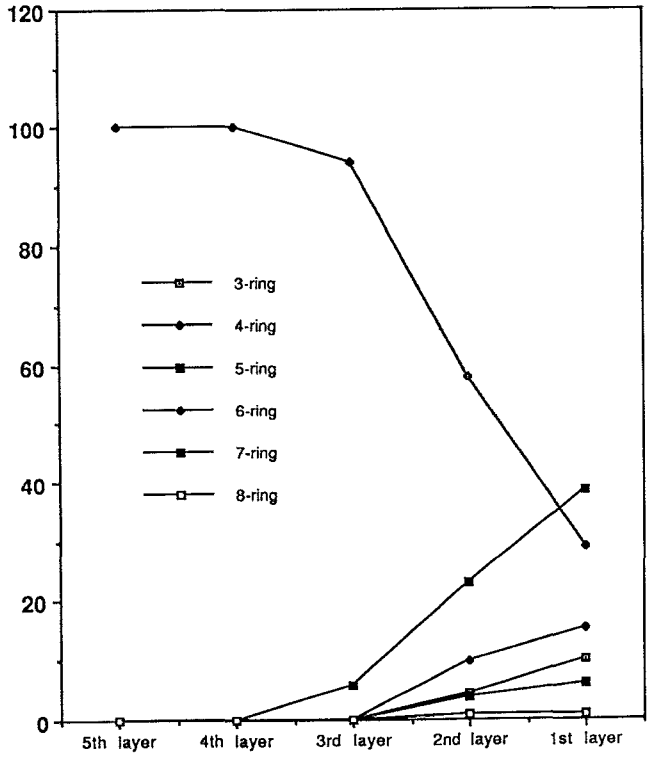

FIG. 2. Ring size distribution profile along the z axis of the a-cristobalite surface.

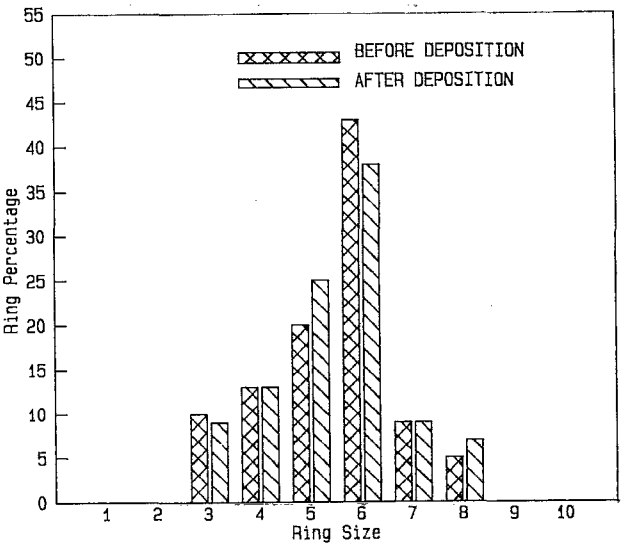

FIG. 4. Ring size distribution, in the top 6 Å region of the glass, before and after the deposition of 250 Pt atoms on the a-quartz relaxed surface.

in the bulk crystal. The intensity of the six-membered rings decreases towards the surface as other ring sizes form. The amorphized quartz showed similar behavior, although quartz contains both six- and eight-membered rings. Although the outer surfaces are reconstructed, the ring size distributions are significantly more narrow than in the glass surfaces. These different glass and amorphized surfaces enable evaluation of adsorption onto amorphous surfaces with broad surface ring size distributions and the amorphized surfaces which have much narrower surface ring size distributions. Figures 3, 4, and 5 show the ring size distributions for top 6 Å of the glass (averaged over the five glass surfaces), amorphized-quartz, and amorphized-cristobalite surfaces, respectively, prior to deposition (as well as after deposition, which will be discussed later). The much narrower distribution on the amorphized surfaces are evident, with the a-cristobalite surface showing the narrowest distribution.

For the simulation of the deposition, one Pt atom at a time was introduced from a random position approximately 5 Å above the free surface. Its initial velocity was sampled from a normal distribution around that corresponding to the 300 K mean velocity value for the adsor-

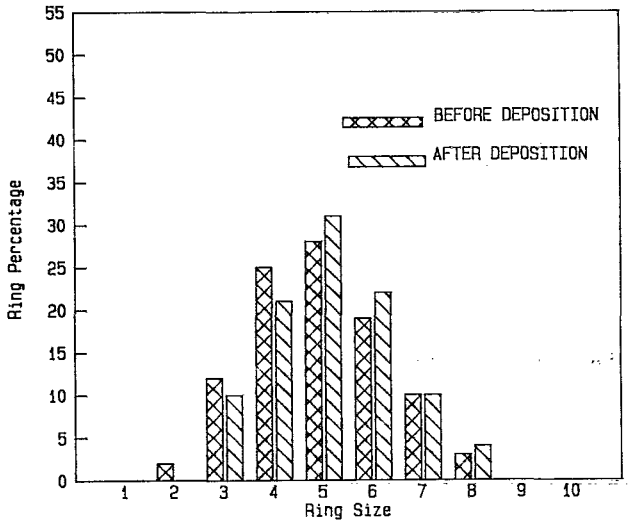

FIG. 3. Ring size distribution, in the top 6 Å region of the glass, before and after the deposition of 250 Pt atoms. All curves represent the average of five silica glass surfaces.

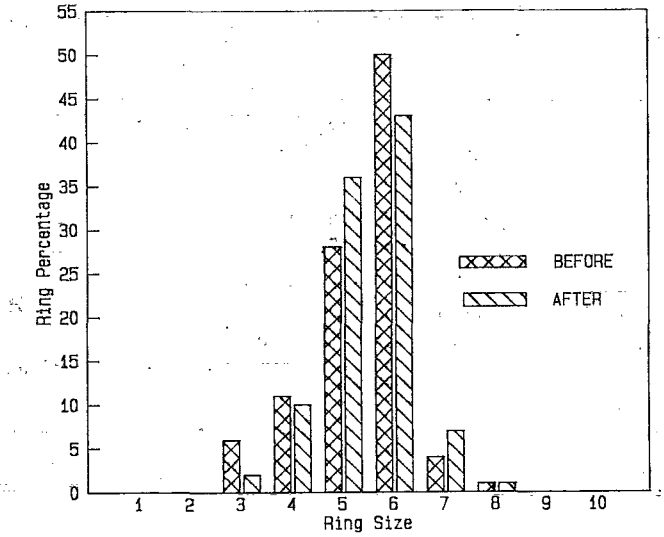

FIG. 5. Ring size distribution, in the top 6 Å region of the glass, before and after the deposition of 250 Pt atoms on the a-cristobalite relaxed surface.

bate. This was achieved by sampling separately each component according to the Box–Muller[24] method. In order to direct the adsorbate atoms towards the surface, the sign of the z component of the initial velocity was biased towards the surface. As the adatom approached the surface, it dropped into the potential well of the substrate atoms, increasing its kinetic energy as it did so. This adatom's kinetic energy was transferred to the substrate atoms during the collisions with them. In a real system, this thermal energy would be dissipated throughout the rest of the substrate atoms. In a small simulation system, especially with immobile atoms at the lower region, this excess energy is not dissipated without additional conditions. Therefore, during the first 500 MD steps of the deposition of each adatom, the velocities of the atoms in the thermal sink region (see Fig. 1) were equilibrated to room temperature, thus making the removal of excess kinetic energy occur in a manner meant to mimic the passage of the thermal wave into the bulk of the substrate. During the equilibration time, the velocities of the atoms inside the equilibration region were scaled every tenth timestep. The equilibration region contained one-third of the substrate atoms closest to the immobile slab (Fig. 1). The system was allowed to evolve without any imposed condition for 500 more steps and then a new atom was added, in which the same equilibration process was employed.

RESULTS AND DISCUSSION

One interesting feature of the simulations was the persistence of the penetration depth of the adsorbates into the substrates, as shown in the upper portions of Figs. 6, 7, and 8, where the initial and final z-axis density profile of the glass, α-quartz, and α-cristobalite substrates, respectively, are shown along with the final z-axis density profile of the Pt atoms. (The potential energy of the substrate-adsorbate system as a function of the z coordinate, before and after the deposition, are also shown in the bottom portion of each figure. The Y axis is conveniently set up to give both energy and density data on the same graph, although obviously the numbers are completely unrelated above and below zero.) In each figure, the free surface is towards the right, between 20–25 Å for the substrate, and the interior of the substrate is towards the left, with the lowest 10 Å of each substrate not being included in the figures. Using a point similar to the location of a Gibb's dividing surface on the number density curve of the substrate and another point similar to placing the Gibb's dividing surface on the inner portion of the number density curve of the Pt atoms, penetration depths between 5 and 6 Å into the glass and amorphized surfaces were measured.

In the beginning of the deposition, the adsorbate atoms approach the surface and interact with the nearest available O. Then they diffuse inside the surface relatively quickly until they find a final binding position. Most of the time another Pt atom was added before the previous one acquired its final place and, consequently, more than one adsorbate atom were moving in the metal-glass interface. The rate of deposition in the simulations, one atom per ps, is orders of magnitude faster than the experimental rates. This simply means that the concentration of Pt atoms in the interface during the simulation increases much more rapidly than during the experiments. Therefore the Pt–Pt attractive interactions start at the very early stages of the formation of the interface and may restrict absorbtion into the subsurface. However, previous simulations of the deposition of just two, well separated, Pt atoms on a silica surface showed that the diffusion depth along the z axis was similar to the results shown here.[11]

The penetration depth of the adsorbates inside the glass appears to be similar to the distance cutoff of their effective interactions (5.5 Å). Truncating just the LJ Pt–O potential to a shorter interaction distance cutoff (3.5 Å), keeping the other interactions at the longer cutoff, resulted in a shorter penetration distance. At first glance, it appears that the adsorbate atoms finally bind when the number of their pairwise attractive interactions reaches a maximum value inside a sphere with radius equal to the effective interaction distance cutoff. A simple interpretation of this inward migration is as follows. An adsorbed atom at the outermost surface receives a net attractive force from the substrate atoms (predominantly oxygen) in the $-z$ direction. Even as the adatom moves into the substrate, as long as there are more neighbors below the adatom than above it in its sphere of interactions, there is a net force downward, assuming all other things being equal. Obviously, all other things are not necessarily equal since closer neighbors have a much greater influence than those farther away and the detailed near neighbor structure, binding energies, activation energies for migration from specific sites, migration paths, and the kinetic energy of a specific adatom all come into play. A shorter Pt–O interaction distance means a smaller driving force into the substrate, especially with additional Pt adsorbing at the outer surface, affecting the previously adsorbed Pt via the longer Pt–Pt attraction. Truncating *all* LJ interactions with Pt to the shorter distance led to a penetration distance similar to that reported in this paper. Clearly, a more in-depth analysis will be necesssary in order to sort out these different effects. Nonetheless, when the net conditions are fulfilled for the adatoms, they stop moving inward. At the later stages of the deposition, adatoms stay at the outer surface forming a continuous layer, with the adatom/substrate interface no longer moving inward. There appears to be a limit to the number of adatoms which can enter the substrate surface. The final arrangement must correspond to a local minimum of the total energy, whose barriers do not allow for the system to move to a more global minimum, at least during the time of the simulation.

The analysis of the ring size distribution before and after the deposition shows an increase in the number of the five-, six-, seven-, and eight-membered rings and a decrease in the number of the two-, three-, and four-membered rings on the glass substrates (Fig. 3). The amorphized surfaces showed similar behavior except for a reduction in the six-membered rings. There may be a correlation between the concentration of smaller rings and penetration depth, since the penetration depth is slightly greater in the amorphized surfaces than in the glasses.

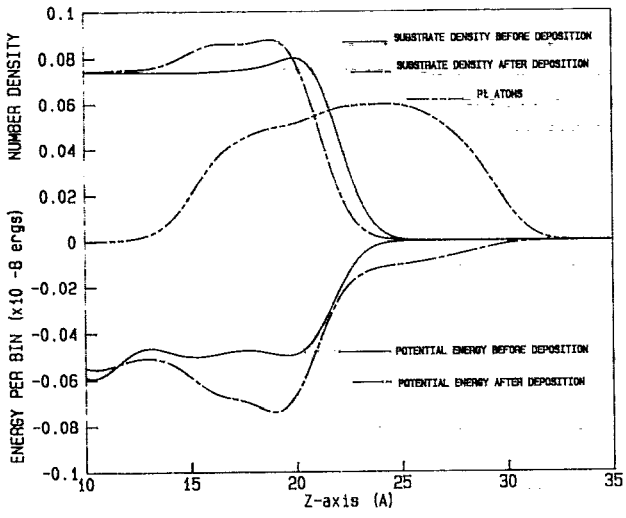

FIG. 6. Number density and total potential-energy profiles along the z axis of substrate and absorbates before and after the deposition of 250 Pt atoms. All curves represent the average of five silica glass surfaces. In Figs. 6, 7, and 8 the substrate interior starts to the left (0–10 Å of interior not included in figures), and the substrate surfaces are at 20–25 Å, with the original gas phase at the right.

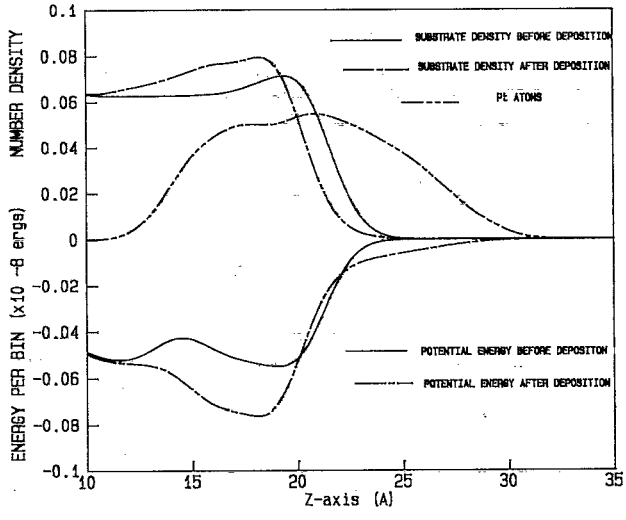

FIG. 8. Number density and total potential-energy profiles along the z axis of substrate and absorbates before and after the deposition of 250 Pt atoms on the a-cristobalite relaxed surface (also see Fig. 6).

The deposition of the adsorbates caused a compression along the normal to the interface direction. Using a Gibbs dividing surface for the substrate, the average compression for the five glass surfaces was approximately equal to 0.9 Å, with clearly greater values for the a-quartz and a-cristobalite surfaces (Figs. 6–8). The differences in the Pt number density profile along the z axis are associated with the differences in the surface area of these systems.

There is a minimum in the potential energy (maximum of the cohesive energy) close to the middle of the metal-glass interface (bottom portions of each graph in Figs. 6, 7, and 8). This can be interpreted in terms of the increase of the total density in this region. Although not shown here, the energy per particle as a function of the z component does not possess any characteristic minimum. Therefore, the total potential-energy minimum is the result of the increased number of bonds per unit volume in this region.

The bond-angle analysis shows that the distribution of the O–Si–O angles around the tetrahedral angle (109.471°) became slightly broader after the deposition (Fig. 9). In the case of the glass surfaces and the a-cristobalite surface, the broadening is symmetrical to the initial distribution. In the a-quartz surface, there is a small shift of the final distribution to higher values.

The changes in the Si–O–Si bond-angle distribution in the interfaces after the deposition are shown in Fig. 10. In all cases the distribution after the deposition was shifted towards smaller values than before the deposition. Smaller values for the Si–O–Si angles generally correspond to

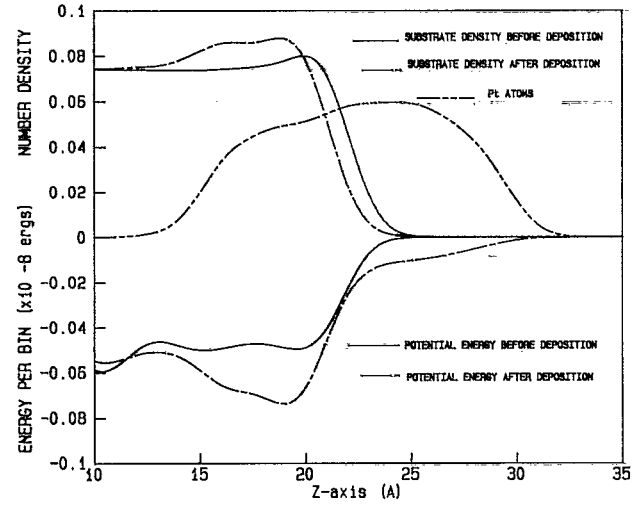

FIG. 7. Number density and total potential-energy profiles along the z axis of substrate and absorbates before and after the deposition of 250 Pt atoms on the a-quartz relaxed surface (also see Fig. 6).

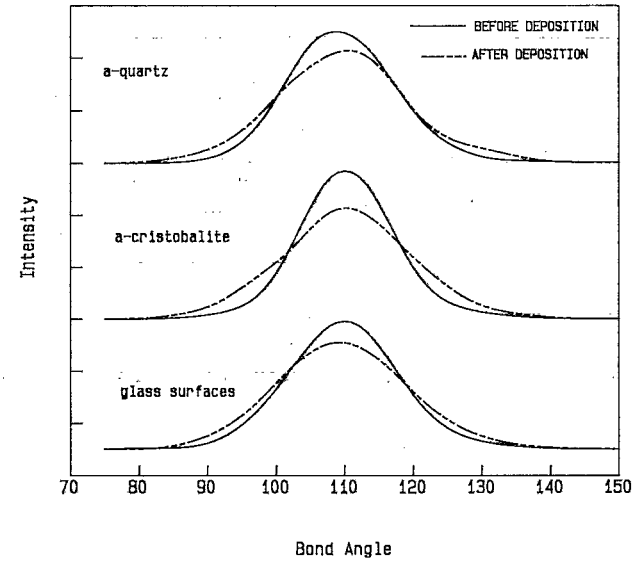

FIG. 9. O–Si–O bond-angle distribution, in the top 6 Å region of the glass, before and after the deposition of 250 Pt atoms.

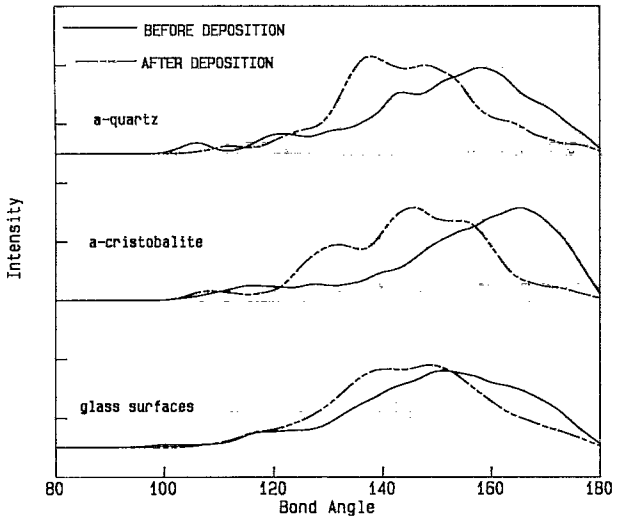

FIG. 10. Si–O–Si bond-angle distribution, in the top 6 Å region of the glass, before and after the deposition of 250 Pt atoms.

smaller rings. However, the ring size distribution analysis showed that there was a small decrease in the percentage of small rings and a relative increase in the percentage of larger rings in all studied systems (Figs. 3, 4, and 5), opposite to what might be inferred from the Si–O–Si bond-angle analysis. This shift in the Si–O–Si angle is the result of the deformation of the rings caused by the presence of the adatoms. Oxygen ions which had their Si–O–Si bond angle shifted to values smaller than 150° remained in the five- and six-membered rings which they had been in prior to the deposition. Smaller siloxane bond angles have been observed in *ab initio* molecular-orbital calculations when a cation is brought near the bridging oxygen of the siloxane bond in the pyrosilicic acid molecule.[25] Based upon the relationship between the siloxane bond angle and Si–O bond length, a smaller bond angle results in longer Si–O bonds, with a concomitant decrease in the strength of the bond at the site, thus making the site more reactive. The simulations therefore show that the adsorbates may alter the reactivity of the silica surface via the formation of smaller bond angles. However, the presence of the Pt in close proximity to the siloxane bonds may inhibit interactions with molecular species which might rupture these bonds (such as water molecules).

CONCLUSIONS

Molecular-dynamics computer simulations of Pt deposition onto silica glass and amorphized quartz and cristobalite surfaces showed absorption of the Pt into subsurface regions and structural modifications of the substrate surfaces. The adsorbate-substrate interfaces had thicknesses of 5–6 Å. All of the surfaces studied here were compressed by about 1 Å after the deposition. There was a significant shift in the Si–O–Si bond angle distribution towards smaller values which was not accompanied by bond fractures or formation of smaller sized rings. Rather, the bond-angle shifts were caused by a distortion of the five- and six-membered rings in the glass surface.

ACKNOWLEDGMENTS

The authors gratefully acknowledge partial support from the National Science Foundation, Grant No. DMR-8907553.

[1] G. Via, H. Sinfelt, and F. Lytle, J. Chem. Phys. **71**, 690 (1979).
[2] S. M. Levine and S. H. Garofalini, Surf. Sci. **163**, 59 (1985).
[3] M. Liehr, F. LeGoues, and G. Rubloff, J. Vac. Sci. Technol. **3**, 983 (1985).
[4] B. Maschhoff, K. Zavadil, and N. Armstrong, Appl. Surf. Sci. **27**, 285 (1986).
[5] M. Liehr, H. Dallaporta, and J. E. Lewis, Appl. Phys. Lett. **58**, 589 (1988).
[6] H. Dallaporta, M. Liehr, and J. E. Lewis, Phys. Rev. B **41**, 5075 (1989).
[7] A. A. Galuska, J. Vac. Sci. Technol. A **9**, 2907 (1991).
[8] C. H. F. Peden, K. B. Kidd, and N. D. Shinn, J. Vac. Tech. A. **9**, 1518 (1991).
[9] R. T. K. Baker, S. J. Tauster, and J. A. Dumesic, in *189th American Chemical Society Annual Meeting*, edited by R. T. K. Baker, S. J. Tauster, and J. A. Dumesic (Washington D.C.: The Society, Miami Florida, 1986), p. 278.
[10] S. M. Levine and S. H. Garofalini, Surf. Sci. **177**, 157 (1986).
[11] S. M. Levine and S. H. Garofalini, J. Chem. Phys. **88**, 1242 (1988).
[12] A. Nordsieck, Math. Comp. **16**, 22 (1962).
[13] B. P. Feuston and S. H. Garofalini, J. Chem. Phys. **89**, 5818 (1988).
[14] R. G. Newell, B. P. Feuston, and S. H. Garofalini, J. Mater. Res. **4**, 434 (1989).
[15] B. F. Feuston and S. H. Garofalini, J. Chem. Phys. **91**, 564 (1989).
[16] D. M. Zirl and S. H. Garofalini, J. Am. Ceram. Soc. **73**, 2848 (1990).
[17] B. P. Feuston and S. H. Garofalini, J. Appl. Phys. **68**, 4830 (1990).
[18] B. F. Feuston and S. H. Garofalini, Chem. Phys. Lett. **170**, 264 (1990).
[19] H. Melman and S. H. Garofalini, J. Non-Cryst. Solids **134**, 107 (1991).
[20] S. H. Garofalini, in *Structure and Bonding in Non-Crystalline Solids*, edited by G. E. Walrafen and A. G. Revesz (Plenum, New York, 1986), pp. 1–12.
[21] S. H. Garofalini and D. M. Zirl, J. Vac. Sci. Technol. A **6**, 975 (1988).
[22] F. H. Stillinger and T. A. Weber, Phys. Rev. B **31**, 5262 (1985).
[23] S. Levine and S. Garofalini, Surf. Sci. **167**, 198 (1986).
[24] W. H. Press, B. P. Flannery, S. A. Teukolsky, and W. T. Vetterling, *Numerical Recipes* (Cambridge University Press, Cambridge, 1988).
[25] K. L. Geisinger, G. V. Gibbs, and A. Navrotsky, Phys. Chem. Minerals **11**, 266 (1985).